Quaternion-Michelson Descriptor for Color Image Classification

Rushi Lan and Yicong Zhou, *Senior Member, IEEE*

***Abstract*— In this paper, we develop a simple yet powerful framework called *quaternion-Michelson descriptor (QMD)* to extract local features for color image classification. Unlike traditional local descriptors extracted directly from the original (raw) image space, QMD is derived from the *Michelson contrast* law and the *quaternionic representation (QR)* of color images. The Michelson contrast is a stable measurement of image contents from the viewpoint of human perception, while QR is able to handle all the color information of the image holisticly and to preserve the interactions among different color channels. In this way, QMD integrates both the merits of Michelson contrast and QR. Based on the QMD framework, we further propose two novel *quaternionic Michelson contrast binary pattern* descriptors from different perspectives. Experiments and comparisons on different color image classification databases demonstrate that the proposed framework and descriptors outperform several state-of-the-art methods.**

***Index Terms*— Color image classification, local descriptor, quaternion, Michelson contrast, quaternionic representation (QR).**

I. Introduction

IMAGE classification aims to assign one or multiple labels to a given image according to its content. It is a longstanding research topic in the fields of computer vision and pattern recognition for its numerous applications. A conventional image classification system is usually composed of two crucial components, i.e. image representation and feature matching. The objective of the first component is to extract discriminative and robust characteristics to represent the images. Based on the derived features, feature matching measures the similarity among images and then assigns the labels accordingly.

As a key role in the image classification system, image representation is a challenging task. The major reason lies in that the images, captured from the real complex environments, usually suffer from lots of unwanted variations, including occlusions, background and illumination changes, and different poses. It is even difficult for humans to differentiate images that belong to the same class. A promising image representation algorithm should not only reveal the essential and discriminative characteristics of the image but also be robust to all kinds of variations.

A. Related Work

The essential objective of image representation is to find an appropriate way to describe the relations among pixels in an image or a local region. A large number of efforts have been paid to image representation, and plenty of image descriptors have been proposed so far. Based on the portion of image contents used for image representation, the existing image descriptors can be generally classified into two categories: global descriptors and local descriptors. The global descriptors take the whole image content into account to obtain a image representation. Although these descriptors have performed well in several applications, they are heavily dependent on the segmentation results and quite sensitive to background variations. In this work, we focus on local descriptors.

A large number of local descriptors have been proposed from various perspectives. In contrast to global descriptors, local descriptors are derived from local regions such that they capture the micro-structure characteristics of the image. Representative local descriptors, such as scale-invariant feature transform (SIFT) [1], affine-SIFT (ASIFT) [2], speeded up robust features (SURF) [3], and local binary pattern (LBP) [4], have achieved great success in face recognition, texture classification, and image retrieval. In order to further improve the discriminative capacity of local descriptors, several supplementary properties of the image have been taken into account. Because gradient information reveals the change rate of the local color distribution in an image, it has been applied to design local descriptors. The histograms of oriented gradient (HOG) descriptor [5] is an important image representation using the gradient feature. Following this idea, many gradient-based local descriptors have been proposed [6], [7]. Similar to the gradient, image edges have also been introduced to derive local descriptors. The local edge histogram descriptor (EDH), which is the statistics of different edge types, was designed for image matching [8], [9]. The edge feature is also coupled with LBP to derive local maximum edge binary patterns for image retrieval and object tracking [10]. Similarly, Satpathy *et al.* developed the discriminative robust local binary pattern (DRLBP) and ternary pattern (DRLTP) to apply the edge and texture information for object recognition [11]. Unlike the aforementioned strategies, several researchers recently developed local descriptors applying the human

Manuscript received November 9, 2015; revised May 8, 2016, June 13, 2016, and August 23, 2016; accepted August 30, 2016. Date of publication September 2, 2016; date of current version September 16, 2016. This work was supported in part by the Macau Science and Technology Development Fund under Grant FDCT/106/2013/A3 and in part by the Research Committee at University of Macau under Grant MYRG2014-00003-FST and Grant MYRG2016-00123-FST. The associate editor coordinating the review of this manuscript and approving it for publication was Prof. Weisi Lin. *(Corresponding author: Yicong Zhou.)*

The authors are with the Department of Computer and Information Science, University of Macau, Macau 999078, China (e-mail: rslan2012@gmail.com; yicongzhou@umac.mo).

Color versions of one or more of the figures in this paper are available online at http://ieeexplore.ieee.org.

Digital Object Identifier 10.1109/TIP.2016.2605922

perception principle in the extracting procedure. For example, several Weber local descriptors (WLDs) have been proposed following the Weber's law [12] that is a special contrast measurement of the image content to reflect the local characteristics. They have improved performance in various applications [13]–[16].

Because the color image consists of different color channels, a common way to obtain the color image representation is to extract the aforementioned global/local descriptors from each color channel individually, and then concatenate them together to form a feature vector. However, this way neglects the interaction among the color channels. To overcome this problem, researchers develop the descriptors using the *quaternionic representation (QR)* of color images. QR is a simple and elegant representation that encodes all the color components of a color pixel into a quaternion [17]. It possesses several attractive merits for color image processing, such as holistically processing all color channels [18], [19], having relatively lower computation complexity compared with other vector representation algorithms [20], and achieving the vector cross correlation [21], etc. Due to these advantages, several quaternionic descriptors have been proposed, including the quaternionic Zernike moment descriptors [22], [23], quaternionic Fourier-Mellin moment [24] and its orthogonal version [25], geometric Fourier descriptor [26], hypercomplex polar Fourier descriptor [27], quaternion moment descriptors [28], and quaternion pseudo-Zernike moment [25], etc. These descriptors are extensions of the corresponding complex moments and are global representations of the color image. They suffer from the same problem as the global descriptors. Very little attention has been paid on extracting the local descriptors based on QR. In our previous work, we extended LBP to the quaternion domain, and proposed the quaternionic LBP (QLBP) [29] and quaternionic local ranking binary pattern (QLRBP) [30]. QLBP first performs a Clifford translation to the QR matrix, and then conducts the traditional LBP on the phase image of the transformed result. QLRBP improves QLBP by bringing ranking concept to the quaternion domain and conducting LBP to a weighted L_1 phase. These two descroptors take the advantages of both QR and LBP, and achieve satisfactory performance for different applications.

B. Our Main Contributions

In this paper, we propose a novel framework called *quaternion-Michelson descriptor (QMD)* for color image classification. QMD derives the local descriptors of color images in the quaternion domain using the Michelson contrast. Compared with the Weber's law, the Michelson contrast [31] is a more stable measurement of the human perception of the image content [32]. The QR-based Michelson contrast takes relations among different color channels into account to describe the the perception of color images. Integrating the QR and Michelson contrast, QMD combines both of their advantages to provide a discriminative representation of the color image. Using the proposed QMD framework, as examples, we develop two *quaternionic Michelson contrast binary pattern (QMCBP)* descriptors. They extract the Michelson contrast of color images in the quaternion domain from different perspectives. A number of experiments are conducted to evaluate the proposed descriptors using different applications, and comparison results validate their effectiveness. Our main contributions are summarized as follows:

- We propose a simple yet very powerful *Quaternion-Michelson Descriptor (QMD)* framework for color image classification. To the best of our knowledge, this is the first time to derive local descriptors of color images using the Michelson contrast in the quaternion domain. QMD benefits both advantages of Michelson contrast and QR.
- Based on the proposed QMD framework, we develop two novel *quaternionic Michelson contrast binary pattern (QMCBP)* descriptors as examples. They extract the Michelson contrast of color images from different perspectives.
- Extensive experiments are carried out to evaluate the QMCBP performance for different color image classification applications. The comparison results show that the proposed QMCBPs outperform several state-of-the-art local descriptors.

The rest of this paper is organized as follows: Section II presents related preliminary knowledge. Section III describes the proposed QMD framework in detail. Section IV presents two novel QMCBP descriptors using the QMD framework. Section V evaluates the proposed descriptors for different color image classification applications. Section VI draws a conclusion.

II. Preliminaries

As preliminary knowledge, this section briefly presents the Michelson contrast, quaternion algebra, and quaternionic representation (QR).

A. Michelson Contrast

Image contrast measures the luminant difference between a target and its surroundings, and it is considered as a fundamental perceptual attribute of an image. The Michelson contrast is a bounded and stable measurement of the image. Suppose Ω is a local region in an image. The Michelson contrast of Ω is defined as [31]:

$$\xi_\Omega = \frac{I_{\max} - I_{\min}}{I_{\max} + I_{\min}}, \tag{1}$$

where $I_{\max}$ and $I_{\min}$ represent the maximum and minimum values within region Ω respectively. The result of ξ_Ω depends on the values of $I_{\max}$ and $I_{\min}$ as follows:

$$\xi_\Omega = \begin{cases} 1, & \text{if } I_{\max} > I_{\min} = 0; \\ (0, 1), & \text{if } I_{\max} > I_{\min} > 0; \\ 0, & \text{if } I_{\max} = I_{\min}. \end{cases} \tag{2}$$

We set $\xi_\Omega = 0$ if $I_{\max} = I_{\min} = 0$. Eqs. (1)-(2) indicate that ξ_Ω is a relative contrast measurement of Ω rather than the absolute contrast like $I_{\max} - I_{\min}$. For different regions, the normalized coefficient $I_{\max} + I_{\min}$ will differ. As a result, ξ_Ω contains more comprehensive local characteristics in contrast with $I_{\max} - I_{\min}$. ξ_Ω is an optimal contrast measurement

of Ω in the case that the bright and dark characteristics are equally presented [33], [34].

B. Quaternion Algebra

Mathematically, quaternion is an associative but not commutative algebra over $\Re$, which was first developed by Hamilton in 1843 [35]. The quaternion number system can be presented as follows:

$$\mathbb{H} = \{q_0 + iq_1 + jq_2 + kq_3 \mid q_n \in \Re, n = 0, 1, 2, 3\}, \quad (3)$$

where i, j and k are the basic complex operators, and they satisfy the following relations:

$$i^2 = j^2 = k^2 = ijk = -1, \quad (4)$$

$$ij = -ji = k, jk = -kj = i, ki = -ik = j. \quad (5)$$

For a quaternion $\dot{q} = q_0 + iq_1 + jq_2 + kq_3$, q_0 is called the real part of $\dot{q}$, while $iq_1 + jq_2 + kq_3$ is its imaginary part. If $q_0 = 0$, $\dot{q}$ becomes a pure quaternion. The conjugate, modulus, and inverse operations of $\dot{q}$ are defined as follows respectively:

$$\dot{q}^* = q_0 - (iq_1 + jq_2 + kq_3), \quad (6)$$

$$|\dot{q}| = \sqrt{q_0^2 + q_1^2 + q_2^2 + q_3^2}, \quad (7)$$

$$\dot{q}^{-1} = \frac{\dot{q}^*}{|\dot{q}|^2}. \quad (8)$$

Except for the algebraic form in Eq. (3), $\dot{q}$ can also be represented in the polar form as follows:

$$\dot{q} = |\dot{q}|e^{\dot{z}\theta} = |\dot{q}|(\cos\theta + \dot{z}\sin\theta), \quad (9)$$

where $\dot{z} = \frac{iq_1 + jq_2 + kq_3}{\sqrt{q_1^2 + q_2^2 + q_3^2}}$ and $\theta = \arctan\frac{\sqrt{q_1^2 + q_2^2 + q_3^2}}{q_0}$. $\dot{z}$ and θ are known as the eigenaxis and phase of $\dot{q}$ respectively. A four quadrant arctangent (atan2) is used to calculate θ. In the following, we exploit $\theta(\cdot)$ as an operator to calculate the phase of a quaternion.

One important property of the quaternion algebra is the Clifford translation of quaternion (CTQ) [36]. Let $\dot{p}$ be a unit quaternion. The right Clifford translation of $\dot{q}$, denoted by $\mathrm{CTQ}_r(\dot{q}, \dot{p})$, is defined as:

$$\mathrm{CTQ}_r(\dot{q}, \dot{p}) = \dot{q}\dot{p}. \quad (10)$$

Similarly, we can obtain the left Clifford translation of $\dot{q}$ as $\mathrm{CTQ}_l(\dot{q}, \dot{p}) = \dot{p}\dot{q}$. Note that the CTQ of two pure quaternions is not a pure quaternion in general. $\mathrm{CTQ}_r(\dot{q}, \dot{p}) \neq \mathrm{CTQ}_l(\dot{q}, \dot{p})$ but their phases are identical. The phase of the CTQ result measures the similarity between $\dot{q}$ and $\dot{p}$, and it has been applied to derived the QLBP [29] and QLRBP descriptors [30]. $\dot{p}$ is called reference quaternion of $\dot{q}$ in the CTQ transform.

C. Quaternion Representation (QR)

To handle the color image in the quaternion domain, the first step is to represent the image by quaternions. The color image is usually described in an RGB color space that is a 3D space, while the quaternion is a 4D number system. To deal with this mismatch between the color space and the quaternion domain, the imaginary part of a quaternion is used to represent a color pixel [18]:

$$\dot{F}(x, y) = iR(x, y) + jG(x, y) + kB(x, y), \quad (11)$$

where $\dot{F}(x, y)$ is QR of the color pixel, and $R(x, y)$, $G(x, y)$, and $B(x, y)$ are the red, green, and blue components of a color pixel respectively.

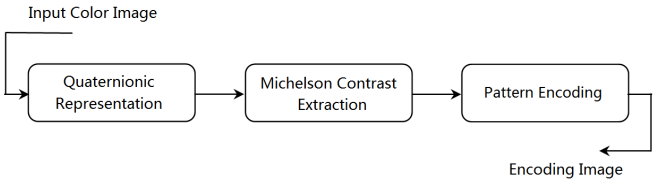

Fig. 1. A schematic picture of Quaternion-Michelson descriptor (QMD).

III. Quaternion-Michelson Descriptor Framework

This section introduces the proposed Quaternion-Michelson Descriptor (QMD) framework in detail. The fundamental of QMD is to extract the Michelson contrast of color images in the quaternion domain. The QR-based Michelson contrast is a novel perception of color images. It simultaneously describes the local contrast and considers the relations among different color components. The features, extracted from this new perception, are expected to contain more informative and discriminative characteristics of color images. Fig. 1 shows the framework of QMD. For a given color image, QMD includes three components, i.e., quaternionic representation (QR), Michelson contrast extraction, and pattern encoding.

A. Quaternionic Representation (QR)

Unlike traditional color image representation methods, QR encodes all color channels of the image using a quaternion in Eq. (11). $\dot{F}(x, y)$ gives a one-to-one mapping between the quaternion domain and RGB color space. Therefore, the aforementioned quaternionic properties and operators (e.g. modulus, phase, rotation, and CTQ) can be used to process the color image directly. Any operation applied to $\dot{F}(x, y)$ will effect all color channels at the same time. These operations, on the other hand, bring novel perspectives to describe the color image.

B. Michelson Contrast Extraction

This procedure aims to search a stable and discriminative contrast measurement of the image content. In Eq. (1), $I_{\max} - I_{\min}$ captures the largest variation among all pixel pairs in a local region, and it is bounded by normalization with $I_{\max} + I_{\min}$. Moreover, QMD extracts this contrast based on QR such that all color information is considered, and the obtained results contain comprehensive features of the original image.

C. Pattern Encoding

Several descriptors can be extracted from the quaternionic Michelson contrast of an image and exploited as image features. For instance, we can directly extract the dense

local histogram from the Michelson contrast for image classification. Owing to the notable success of image encoding algorithms, we further perform a pattern encoding operation to the quaternionic Michelson contrast of an image to derive local descriptors in this work. Consequently, the obtained features contain sufficient image characteristics and provide improved discriminative capacity.

Following the QMD framework, we will propose a quaternionic Michelson contrast binary pattern (QMCBP) in the next section.

IV. Quaternionic Michelson Contrast Binary Pattern

In this section, we first introduce two methods to extract the Michelson contrast of the image in the quaternion domain, present the pattern encoding procedure to derive QMCBP, and finally provide several discussions of QMCBP.

A. Michelson Contrast Extraction in Quaternion Domain

The key step of the proposed descriptor is to extract the Michelson contrast in the quaternion domain. Let $\dot{S} = \{\dot{I}_n | n = 1, 2, \cdots, N\}$ be a small region in $\dot{F}(x, y)$, $\dot{I}_n$ is the QR of the corresponding pixel, and N denotes the pixel number in $\dot{S}$.

Eq. (1) indicates that we need to find the maximum and minimum within $\dot{S}$. That is to say, we need to determine a criterion to order the QR elements in $\dot{S}$. Suppose f is an ordering mapping of $\dot{S}$ as follows:

$$f(\dot{S}) = \{\dot{I}_{t_N} | t_n \in \{1, \cdots, N\}, \dot{I}_{t_1} \leq \dot{I}_{t_2} \leq \cdots \leq \dot{I}_{t_N}\}, \quad (12)$$

where $\leq$ denotes the ordering relationship between two quaternions following the given criterion.

It is easy to design such a function f for real numbers. However, to the best of our knowledge, there is no straightforward way to order two quaternions directly. To overcome this obstacle, an intuitive approach is to transform the quaternions into the real domain before ordering. One simple way is to order the quaternions according to their moduli. From the definition of a quaternion, this is equivalent to the L_2-norm of the vector representation of the color image. The relationships between color channels have not been fully considered.

Our previous work has demonstrated that the phase of the CTQ-ed quaternion reveals the relations among different color channels [29]. CTQ is a simple transform of a quaternion, and the phase of the CTQ result can be applied to measure the similarity of two quaternions. In this work, we apply CTQ to order $\dot{S}$.

Suppose $\dot{p}$ is a unit quaternion, and $\dot{S}_{\dot{p}}$ is the CTQ result of $\dot{S}$. Based on the definition of CTQ in Eq. (10), we can achieve:

$$\dot{S}_{\dot{p}} = \{\dot{I}_n \dot{p} | n = 1, 2, \cdots, N\}. \quad (13)$$

The right Clifford translation is used here. Note that, similar ordering results can be obtained using left Clifford translation to $\dot{S}$. Next, we compute the phase of each element in $\dot{S}_{\dot{p}}$ as follows:

$$\mathbf{\Phi} = \{\phi_n | \phi_n = \theta(\dot{I}_n \dot{p}), n = 1, 2, \cdots, N\}. \quad (14)$$

Note that we will obtain the same $\mathbf{\Phi}$ applying the left Clifford translation. As aforementioned, ϕ_n describes the similarity between $\dot{I}_n$ and $\dot{p}$. Now, $\mathbf{\Phi}$ can be sorted in an ascending or descending order because $\phi_n \in [0, \pi]$. Denote the sorted phase array by $\mathbf{\Phi}'$, which can be presented by:

$$\mathbf{\Phi}' = \{\phi_{t_n} | \phi_{t_1} \leq \phi_{t_2} \leq \cdots \leq \phi_{t_N}, t_n \in \{1, 2, \cdots, N\}\}, \quad (15)$$

where t_n is the element index in $\dot{S}$. Based on $\mathbf{\Phi}'$, we propose two types of Michelson contrast in the quaternion domain as follows.

1) Quaternionic Michelson Contrast Extraction: Once t_n is available, we can order the elements in $\dot{S}$ as follows:

$$\dot{S}' = \{\dot{I}_{t_n} | t_n \in \{1, 2, \cdots, N\}, \phi_{t_1} \leq \phi_{t_2} \leq \cdots \leq \phi_{t_N}\}. \quad (16)$$

$\dot{I}_{t_1}$ is considered as the minimum in $\dot{S}$, while $\dot{I}_{t_N}$ is the maximum. $\dot{I}_{t_1}$ and $\dot{I}_{t_N}$ have the minimal and maximum similarities with $\dot{p}$. If we directly substitute $\dot{I}_{t_1}$ and $\dot{I}_{t_N}$ into Eq. (1), ξ is still a quaternion which is inconvenient for further processing. Because the phase of a quaternion describes the relationship between its components, the Michelson contrast of $\dot{S}$ is defined as follows:

$$\xi_{\dot{S}} = \theta\left(\frac{\dot{I}_{t_N} - \dot{I}_{t_1}}{\dot{I}_{t_N} + \dot{I}_{t_1}}\right). \quad (17)$$

To provide a deeper insight, we analyze $\xi_{\dot{S}}$ with all color components. Let $\dot{p} = i R_{t_0} + j G_{t_0} + k B_{t_0}$, $\dot{I}_{t_1} = i R_{t_1} + j G_{t_1} + k B_{t_1}$, and $\dot{I}_{t_N} = i R_{t_N} + j G_{t_N} + k B_{t_N}$, where $\{R_{t_0}, G_{t_0}, B_{t_0}\}$, $\{R_{t_1}, G_{t_1}, B_{t_1}\}$, and $\{R_{t_N}, G_{t_N}, B_{t_N}\}$ are the corresponding color intensities of $\dot{p}$, $\dot{I}_{t_1}$, and $\dot{I}_{t_N}$, respectively. Based on the definition of Michelson contrast, it has

$$\frac{\dot{I}_{t_N} - \dot{I}_{t_1}}{\dot{I}_{t_N} + \dot{I}_{t_1}} = \frac{i\Delta_R + j\Delta_G + k\Delta_B}{i\Theta_R + j\Theta_G + k\Theta_B}, \quad (18)$$

where $\Delta_R = R_{t_N} - R_{t_1}$, $\Delta_G = G_{t_N} - G_{t_1}$, $\Delta_B = B_{t_N} - B_{t_1}$, $\Theta_R = R_{t_N} + R_{t_1}$, $\Theta_G = G_{t_N} + G_{t_1}$, and $\Theta_B = B_{t_N} + B_{t_1}$. Note that $\dot{I}_{t_N}$ and $\dot{I}_{t_1}$ are two most dissimilar pixels by taking $\dot{p}$ as the reference quaternion. Δ_R, Δ_G, and Δ_B represent the differences of corresponding color components between these two color pixels. Θ_R, Θ_G, and Θ_B measure their total intensities. Denote $\{\Delta_R, \Delta_G, \Delta_B\}$ and $\{\Theta_R, \Theta_G, \Theta_B\}$ by $\mathbf{\Delta}$ and $\mathbf{\Theta}$. Substituting Eq. (18) into Eq. (17) yields

$$\xi_{\dot{S}} = \arctan \frac{\sqrt{(\Delta_G\Theta_B - \Delta_B\Theta_G)^2 + (\Delta_B\Theta_R - \Delta_R\Theta_B)^2 + (\Delta_R\Theta_G - \Delta_G\Theta_R)^2}}{(\Delta_R\Theta_R + \Delta_G\Theta_G + \Delta_B\Theta_B)} \quad (19)$$

We can observe that $\xi_{\dot{S}}$ applies the interactions between $\mathbf{\Delta}$ and $\mathbf{\Theta}$ to describe the local contrast. If $\mathbf{\Delta}$ is similar to $\mathbf{\Theta}$, the numerator of $\xi_{\dot{S}}$ will be small, and the denominator will be large because it is analogous to the inner product of two vectors. $\xi_{\dot{S}}$ will be a small value in this situation. Otherwise, $\xi_{\dot{S}}$ will be large. Compared with color intensities, $\mathbf{\Delta}$ and $\mathbf{\Theta}$ are simple features of the local region from different perspectives, and their combination in Eq. (19) provides a more informative view of the image content. Considering another reference quaternion $\dot{p}$ in CTQ, we may obtain another Michelson contrast result for feature extraction.

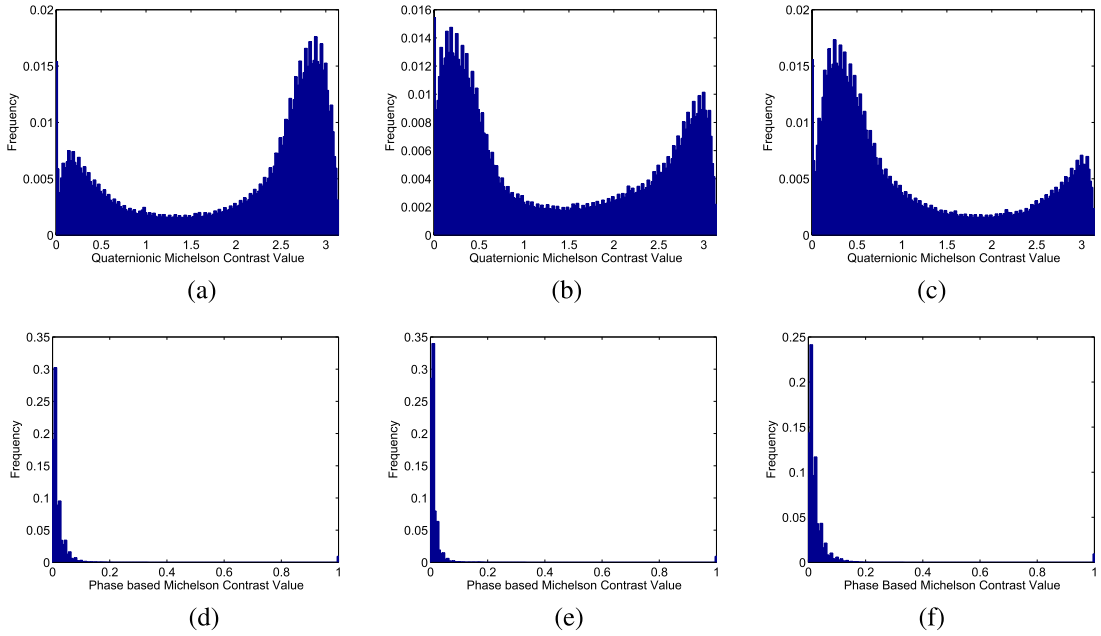

Fig. 2. Distributions of different QR-based Michelson contrasts. (a)-(c) are the distribution results of quaternionic Michelson contrast derived by using i, j, and k in CTQ respectively, and (d)-(f) are corresponding results of phase-based Michelson contrast.

2) Phase-Based Michelson Contrast Extraction: In Eq. (17), to derive $\xi_{\dot{S}}$, we need to find $\{\dot{I}_{t_1}, \dot{I}_{t_N}\}$ and compute the phase. In fact, $\mathbf{\Phi}$ in Eq. (14) contains discriminant information of the original image and has been successfully applied to derive the local descriptor [29]. Here we propose a simplified version of $\xi_{\dot{S}}$ as follows:

$$\xi'_{\dot{S}} = \frac{\phi_{t_N} - \phi_{t_1}}{\phi_{t_N} + \phi_{t_1}}. \tag{20}$$

$\xi'_{\dot{S}}$ actually is the result of directly performing Eq. (1) in the phase image. ϕ_{t_n} is a similarity measurement of $\dot{I}_{t_n}$ and $\dot{p}$, which emphasizes a specific characteristic of the original color image. $\xi'_{\dot{S}}$ here is a similarity-based contrast, and can be considered as a higher level representation of color images.

B. Pattern Encoding

From Eqs. (17) and (20), it is not difficult to find that $\xi_{\dot{S}} \in [0, \pi]$ and $\xi'_{\dot{S}} \in [0, 1]$. It is interesting to study the distributions of proposed contrasts in natural images. To this end, we collect an image set that consists of face, texture, and pedestrian images, and the total number of images is about ten thousands. As shown in Eq. (14), we apply the phase of the CTQ result to derive the quaternionic Michelson contrast. Three complex operators, i, j, and k, are applied in CTQ. We use the histograms to illustrate distributions of two proposed contrasts. The average histograms of all images in the image set are plotted in Fig. 2, where (a)-(c) are the distribution results of quaternionic Michelson contrast derived by using i, j, and k in CTQ, and (d)-(f) are corresponding results of phase-based Michelson contrast. For quaternionic Michelson contrast, each distribution is similar to a mixture of two Gaussian distributions. On the other hand, we can observe that about 95% of the phase-based Michelson contrast lie in the region $[0, 0.1]$. Their distributions are similar to those distributions of luminance in natural scenes [37], namely they are all skewed toward the low end of the range. Hence, if we directly use the histogram of $\xi'_{\dot{S}}$ as the descriptors of color images, the derived features may lack discriminative characteristics to distinguish different images.

To address this problem, we further introduce an encoding procedure to the proposed Michelson contrasts. Because the well-known local binary pattern (LBP) has been proven to be simple and effective, and has wide applications, in this work, we implement LBP in the quaternionic Michelson contrast image to derive a more powerful descriptor. The uniform LBP is selected here for its excellent performance in texture classification and face recognition. Combining the Michelson contrast and the definition of LBP, we propose a local descriptor called *quaternionic Michelson contrast binary pattern (QMCBP)* as follows:

$$\text{QMCBP}_{P,R} = \begin{cases} l\left(\sum_{n=0}^{P-1} \delta(\xi_n - \xi_c)2^n\right), & \text{if } H \leq 2, \\ P(P-1)+2, & \text{otherwise,} \end{cases} \tag{21}$$

where $H = |\delta(\xi_{P-1} - \xi_c) - \delta(\xi_0 - \xi_c)| + \sum_{n=1}^{P-1} |\delta(\xi_n - \xi_c) - \delta(\xi_{n-1} - \xi_c)|$ and $\delta(x) = \begin{cases} 1, & x \geq 0. \\ 0, & x < 0. \end{cases}$ ξ_c is the center pixel of a local region in the quaternion Michelsonic contrast of a color image, and $\{\xi_0, \cdots, \xi_{P-1}\}$ are surrounding ones of ξ_c. P is the number of used surrounding pixels of ξ_c, while R is the distance between ξ_n and ξ_c. $l(\cdot)$ is an indexing function that assigns a particular index to each of the uniform patterns [4]. A histogram can be obtained from the QMCBP encoding result and applied as the feature vector for classification. A summary of the QMCBP descriptor extraction is presented in **Algorithm 1**.

Algorithm 1 QMCBP Feature Extraction

Input: The color image F, L reference quaternions $\{\dot{p}_1, \cdots, \dot{p}_L\}$, and the parameters P and R for QMCBP encoding.

- Step 1: Obtain $\dot{F}$, the QR of F, according to Eq. (11).
- Step 2: For $n = 1$ to L, do
  - (a) Conduct CTQ to $\dot{F}$ using $\dot{p}_n$, and then calculate the phase.
  - (b) Extract the Michelson contrast based on the phase according to Eq. (17) or (20).
  - (c) Perform QMCBP encoding to the Michelson contrast with parameters P and R using Eq. (21).
  - (d) Calculate the normalized histogram ρ_n from the QMCBP encoding result .

Output: The QMCBP feature vector of F: $\{\rho_1, \cdots, \rho_L\}$.

C. Discussion

To further clarify the significance of the proposed descriptor, this section analyzes the invariance of QMCBP against different types of changes, and discusses the differences between our QMCBP method and existing related algorithms.

1) Invariance Against Types of Changes: In [38], van de Sande *et al*. studied the invariance of different descriptors against five types of changes: light intensity change, light intensity shift, light intensity change and shift, light color change, and light color changes and shift. As shown in Eq. (1), the Michelson contrast involves the sum operation such that the proposed QMCBP descriptors cannot remove the shift changes. Note that all color channels are scaled by different factors in light color change. This change will yield a new Michelson contrast. As a result, the QMCBP descriptors are sensitive to light color change. The light intensity change, which scales all color channels by the same factor, can be removed by the division operation in Eq. (1), and thus the QMCBP descriptors are invariant to this change.

2) Difference From Methods Using RGB Channels Individually: To derive descriptors for color images, a common way is to extract the descriptors from each color channel individually, and then concatenate them together to form a feature vector. This strategy will ignore the interrelations between color channels. In contrast, the proposed QMCBP is based on QR of color images such that all color channels are considered holistically and processed simultaneously. Hence, QMCBP contains more color information for classification.

3) Difference From LBP: Both LBP and QMCBP include a binary encoding procedure, but their encoding operations are implemented on different objects. For LBP, it directly handles the raw image intensity to derive the local differences for encoding. On the other hand, QMCBP performs the encoding to the image contrast in the quaternion domain. The image contrast is a high level representation of the original image which highlights the edge and texture characteristics of images. This ensures that the derived descriptors to be robust and contain more distinctive features.

4) Difference From WLD [14]: Although WLD and QMCBP both apply the image contrast for representation, they are based on different types of contrasts, and handle the contrast in different manners. WLD uses the histogram of the Weber contrast as features directly. On the other hand, QMCBP further performs an encoding operation to the Michelson contrast in the quaternion domain, and then extracts the histogram of encoding results as local descriptors. The Michelson contrast and encoding operations ensure that the derived QMCBP features reflect the essential characteristics of the original image.

5) Difference From QLRBP [30]: Although both QMCBP and QLRBP use CTQ and LBP operations to derive local descriptors, the use of Michelson contrast yields following differences between QMCBP and QLRBP: (1) QLRBP directly employs the weighted L_1 phase as the input for the LBP encoding, while QMCBP applies the phase to determine an ordering relation for Michelson contrast extraction. (2) The proposed Michelson contrasts contain more discriminative characteristics than the weighted L_1 phase. The phase used in QLRBP is directly derived from the raw pixel intensity values. For QMCBP, $\{\Delta_R, \Delta_G, \Delta_B\}$, $\{\Theta_R, \Theta_G, \Theta_B\}$, and $\{\theta_{t_1}, \theta_{t_N}\}$ are simple features of the local region such that they provide more useful information for feature extraction. (3) QMCBP is more apt to explore local characteristics of images than QLRBP. In QLRBP, all pixels of the image are processed by CTQ with one reference quaternion. This is a global transform of the original image, and may hinder the performance of QLRBP. The proposed QMCBP is able to overcome this limitation. In QMCBP, all elements of $\{\Delta_R, \Delta_G, \Delta_B\}$, $\{\Theta_R, \Theta_G, \Theta_B\}$, and $\{\theta_{t_1}, \theta_{t_N}\}$ adaptively change according to the image content. (4) QMCBP needs fewer parameters than QLRBP. The performance of QLRBP heavily depends on finding the appropriate weights to calculate the phase. There are no such parameters in QMCBP such that it is more convenient to be used for many applications.

V. Experiments and Results

In this section, several experiments will be carried out to demonstrate the effectiveness of the proposed QMCBP descriptors from different perspectives. First, we investigate how the related parameters affect the performance of QMCBP descriptors. Subsequently, the proposed QMCBP descriptors are compared with several state-of-the-art methods in different applications. Finally, a discussion about the time complexity will be given.

A. Effects of Parameters

As aforementioned, we need to determine two types of parameters in the implementation of the QMCBP descriptors, namely the reference quaternions for CTQ and the encoding parameters $\{P, R\}$ in Eq. (21). It is time consuming to test these parameters simultaneously. Alternatively, we first study the effects of different reference quaternions by using fixed $\{P, R\}$. Next, the effects of different settings of $\{P, R\}$ will be evaluated using fixed reference quaternions. The QMCBP descriptor derived from the phase-based Michelson contrast is used here.

1) Effects of Reference Quaternions: One key step in the derivation of QMCBP is to apply reference quaternions to determine the ordering of all elements within a local region. Different reference quaternions will yield different ordering

results and Michelson contrasts. QMCBP derived by a specific reference quaternion may reveal the color characteristic of the image from one view. To achieve a comprehensive descriptor, we collect multi-view QMCBP features by using three reference quaternions becasue the color image is represented in a 3D space. On the other hand, the used reference quaternions should not only have the capacity of revealing the color distribution of the image but also be distinctive with each other. From these perspectives, the following reference quaternions are considered in this work:

1) It is natural to use the three basic complex operators $\{i, j, k\}$ as reference quaternions because any pure quaternion can be represented by their linear combination;
2) The basic complex operator considers the similarity between the image and one color channel at one time. To take more color information into account, we improve the basic complex operators as follows: $\{\frac{i+j}{\sqrt{2}}, \frac{i+k}{\sqrt{2}}, \frac{j+k}{\sqrt{2}}\}$;
3) Inspired by the bag-of-feature (BOF) model, we conduct the fuzzy C-means (FCM) algorithm to the vector representation of the original color image, and use three obtained clusters as the reference quaternions;
4) Applying the BQMP algorithm [39], we can obtain three quaternions from QR of the color image as reference quaternions.

Denote these achieved reference quaternions by RQ_1, RQ_2, RQ_3, and RQ_4, respectively. The corresponding descriptors are represented as QMCBP_1, QMCBP_2, QMCBP_3, and QMCBP_4. In this test, we evaluate the performance of these descriptors by fixing $\{P, R\}$ to $\{8, 1\}$. The pedestrian dataset ETHZ[1] [40] is selected here. It consists of 8580 images for 146 persons in total, and all these images are captured in real complex environments such that there are large variations among images for the same person.

For each image, we extract QMCBP features using RQ_t, $t = 1, \cdots, 4$. To visually illustrate the distributions of the derived features, we utilize the principal components analysis (PCA) method to reduce the dimension of each feature vector to 2, and plot these 2D points in a plane. We use one point to represent each person where each point is the average value of all samples corresponding to the same person. The results are shown in Fig. 3, where (a)-(d) correspond to the features derived by using $\mathrm{RQ}_t, t = 1, \cdots, 4$ respectively. It can be seen that there exist several overlapping points concentrating in the middle of each subfigure. The points in Figs. 3(a) and (b) are more separable than those in Figs. 3(c) and (d). This means that the fixed reference quaternions work better than the ones derived by clustering schemes.

Next, we investigate the proposed QMCBP descriptors with different reference quaternions quantitatively. From the perspective of feature representation, the QMCBP_t descriptors, obtained from RQ_t, are expected to have large similarities within the samples from the same class and small similarities between the samples from different classes. Therefore, the similarities of the pedestrian images in the ETHZ dataset between and within classes are calcualted to quantitatively evaluate the performance of different QMCBP_t descriptors. We apply the following correlation coefficient ρ to measure the similarity between two descriptors $\boldsymbol{v}_1$ and $\boldsymbol{v}_2$:

$$\rho(\boldsymbol{v}_1, \boldsymbol{v}_2) = \frac{\langle \boldsymbol{v}_1 - \bar{v}_1, \boldsymbol{v}_2 - \bar{v}_2 \rangle}{\|\boldsymbol{v}_1 - \bar{v}_1\| \|\boldsymbol{v}_2 - \bar{v}_2\|}, \tag{22}$$

where $\bar{v}_1$ and $\bar{v}_2$ are the mean values of $\boldsymbol{v}_1$ and $\boldsymbol{v}_2$, $\langle \cdot, \cdot \rangle$ denotes the inner product between two vectors, and $\| \cdot \|$ represents the l_2-norm of a vector. For each QMCBP_t descriptor of the images in the database, we compute its similarities between those of the same person and different persons respectively. Table I illustrates the average values of similarities within the same person and between different persons. Denote these two similarities as Γ_w and Γ_b. The ratios of two similarities Γ_w / Γ_b are also given. The larger values of Γ_w / Γ_b indicates that the corresponding descriptors are more suitable for classification.

The results in Table I indicate that QMCBP_3 obtains the most satisfactory within-class similarity, while QMCBP_4 has the worst one. The within-class similarities of QMCBP_1 and QLRBP_2 are quite close. On the other hand, considering the between-classes similarity, QMCBP_4 achieves the best result, while QMCBP_3 performs the worst.

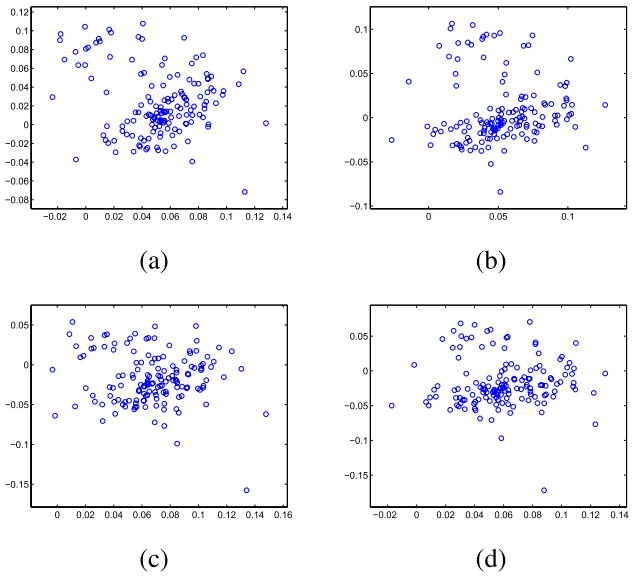

Fig. 3. The 2D distribution of QMCBP descriptors derived by different reference quaternions. These results correspond to following reference quaternions: (a) $\{i, j, k\}$, (b) $\{\frac{i+j}{\sqrt{2}}, \frac{i+k}{\sqrt{2}}, \frac{j+k}{\sqrt{2}}\}$, (c) clustering centers derived by the FCM algorithm, and (d) clustering centers derived by the BQMP algorithm respectively.

TABLE I

AVERAGE SIMILARITIES OF THE QMCBP DESCRIPTORS DERIVED BY DIFFERENT QUATERNION REFERENCES. BEST RESULTS ARE IN BOLD

	QMCBP_1	QMCBP_2	QMCBP_3	QMCBP_4
Γ_w	0.9340	0.9344	**0.9351**	0.9314
Γ_b	0.9028	0.9041	0.9065	**0.9021**
Γ_w/Γ_b	**1.0346**	1.0335	1.0315	1.0325

[1]https://urldefense.proofpoint.com/v2/url?u=https-3A_data.vision.ee.ethz.ch_cvl_aess_dataset_&d=BQIFaQ&c=KXXihdR8fRNGFkKiMQzstu-8MbOxd1NuZkcSBymGmgo&r=-nyP-sC4V4YnLlkugv_yknfikIJobepfWX-TceIc3jI&m=Mmwi0LlsMnQxfviX4ledbpPavP5FE62xW3SVttIm1Po&s=WPoLIeVb6f1yJA5kHBrpVqaZ6xVLpix-wIGDWegs9PU&e=

TABLE II
AVERAGE SIMILARITIES OF THE QMCBP DESCRIPTORS DERIVED BY DIFFERENT ENCODING PARAMETERS. BEST RESULTS ARE IN BOLD FONT

	(8,1)	(12,1.5)	(16,2)	(24,3)
Γ_w	0.9340	0.9110	0.9763	**0.9950**
Γ_b	0.9028	**0.8967**	0.9713	0.9938
Γ_w/Γ_b	**1.0346**	1.0160	1.0051	1.0012

Although QMCBP_3 and QMCBP_4 are both based on adaptive reference quaternions, QMCBP_3 descripotrs are more similar to each other because they gain the highest similarities for within-class and between-classes, while QMCBP_4 descriptors acquire the opposite results. For the descriptors using fixed reference quaternions, QMCBP_2 performs slightly better than QMCBP_1 for within-class similarity, but worse in between-classeses similarity. Considering two similarities together, namely their ratios, the performance of QMCBP_1 surpasses other descriptors. QMCBP_2 is also superior to the two descriptors derived by clustering methods. These results indicate that the fixed reference quaternions are more suitable for QMCBP than those derived by clustering methods. The reason lies in that the clusters of some images usually suffer from large illuminance variations and may be close to each other. As a result, there will be redundant information in the QMCBP descriptors derived by clustering methods. In the following experiments, we select $\text{RQ}_1 = \{i, j, k\}$ as reference quaternions.

2) Effects of Encoding Parameters: The encoding parameters in Eq. (21) also greatly affect the performance of QMCBP descriptors because the QMCBP descriptors derived by different $\{P, R\}$ will differ. Here, we set $\{P, R\}$ to $\{8, 1\}$, $\{12, 1.5\}$, $\{16, 2\}$, and $\{24, 3\}$ as in [4]. The derived QMCBP descriptors are evaluated similarly as in previous experiment, namely the within-class similarity Γ_w and between-class similarities Γ_b are calculated as measurements. Table II illustrates the corresponding results of different parameter pairs.

From Table II, it can be seen that QMCBP is sensitive to the encoding parameters. The parameter pair $\{24, 3\}$ obtains the highest similarities in both situations. This indicates that the derived descriptors lack discriminating information. The descriptors obtained by small parameters show better performance than those with large parameters. Considering two similarities together, the parameter pair $\{8, 1\}$ outperforms other parameter pairs. Thus, it is used in the following experiments.

B. Kinship Verification

Local descriptors are commonly used in various face analysis problems. In this experiment, we choose kinship verification [41] to evaluate the proposed descriptors. Kinship verification aims to determine the following relations for a given face image pair: father-son (F-S), father-daughter (F-D), mother-son (M-S), and mother-daughter (M-D). It is a significant and meaningful research topic to the academic study, and has many potential applications to society.

Two standard testing sets, KinFaceW-I and KinFaceW-II [41], [42], are selected for evaluation here. For the first data set, there are 156, 134, 116, and 127 pairs of facial images for F-S, F-D, M-S, and M-D relations respectively, while the other data set consists of 250 pairs of images for each relation. Note that the two images of each pair in KinFaceW-I data set are obtained from different pictures, and those images in KinFaceW-II data set are acquired from the same picture. Some face image pairs for each kinship relation are shown in Fig. 4. The experiments here are carried out as follows [41], namely the neighborhood repulsed metric learning (NRML) algorithm is used to determine the relation between image pairs for different local descriptors.

Fig. 4. Examples of facial image pairs of different kinship relations in the KinFaceW-II data set. Images from the first to the last rows corresponds to F-S, F-D, M-S, and M-D relations respectively.

The proposed QMCBP descriptors are compared with the following approaches, i.e., LBP [4], WLD [14], LCVBP [43], SIFT [1], SURF [3], QLBP [29], and QLRBP [30] respectively. For LBP and LCVBP methods, we extract the corresponding features from each color channel individually, and then concatenate the obtained descriptors together to form a feature vector. The LCVBP, QLBP, and QLRBP schemes are derived by considering all color information of the image to provide a fair comparison. The QMCBP descriptors derived from the quaternionic Michelson contrast and phase-based Michelson conract are denoted by QMCBP_q and QMCBP_p. All images of each kinship relation are equally divided into five folds. For each fold, all image pairs are considered as positive samples, and the same number of negative pairs are randomly generated. A fivefold cross validation is carried out, and the average verification result is reported. More detailed information can be found in [41]. Table III illustrates the verification performance of all algorithms on different subsets of the two data sets.

For the KinFaceW-I data set, SIFT, SURF, QLRBP, and QMCBP_p achieve more satisfactory performance compared with other methods. For F-S relation, SURF works the best among all features, while SIFT and QLRBP obtain the highest verification results for F-D and M-S relations. QMCBP_p surpasses SIFT and SURF by about four percents in M-D relation. Considering the overall performance, the results of SIFT and QMCBP_p are the same, and SURF slightly outperforms SIFT, QLRBP, and QMCBP_p.

Considering the KinFaceW-II data set, QMCBP_q gains better performance than QMCBP_p for F-S, F-D, and M-S relations. For M-D relation, QMCBP_p and QLBP obtain the identical results. The accuracies of WLD and LCVBP are

TABLE III

VERIFICATION PERFORMANCE (PERCENT) OF DIFFERENT LOCAL DESCRIPTORS ON DIFFERENT SUBSETS OF THE KinFaceW-I AND KinFaceW-II DATA SETS. BEST RESULTS ARE IN BOLD

Methods	KinFaceW-I data set				
	F-S	F-D	M-S	M-D	Mean
LBP [4]	70.5	69.4	68.9	76.0	71.2
WLD [14]	71.2	65.7	68.6	77.7	70.8
LCVBP [43]	69.6	66.9	68.5	73.0	69.5
QLBP [29]	69.9	67.5	68.1	75.7	70.3
QLRBP [30]	73.4	**70.9**	69.4	77.5	72.8
SIFT [1]	75.7	**70.9**	**70.2**	73.6	72.6
SURF [3]	**76.6**	70.6	69.8	74.9	**73.0**
$QMCBP_q$	72.2	68.1	67.8	76.0	71.0
$QMCBP_p$	74.4	69.6	68.6	**77.8**	72.6
Methods	KinFaceW-II data set				
	F-S	F-D	M-S	M-D	Mean
LBP [4]	73.8	68.0	76.6	73.2	72.9
WLD [14]	72.4	71.2	76.2	75.4	73.8
LCVBP [43]	74.8	**71.6**	75.6	73.4	73.9
QLBP [29]	75.2	68.6	76.8	75.6	74.1
QLRBP [30]	76.2	69.8	76.8	**76.2**	74.8
SIFT [1]	74.8	68.4	75.2	74.6	73.3
SURF [3]	76.4	70.2	74.2	71.6	73.1
$QMCBP_q$	**77.2**	**71.6**	**79.0**	73.4	**75.3**
$QMCBP_p$	75.2	71.4	76.6	75.6	74.7

TABLE IV

SUMMARY OF THE TEXTURE IMAGE DATA SETS

Data set name	Num. of class	Num. of each class	Total Num.
KTH-TIPS2-a	11	Vary	4395
KTH-TIPS	10	81	810
USPTex	191	12	2292
Outex TC00013	68	20	1360
Vistex-864	54	16	864

comparable for this data set, and they are better than those of LBP. QLBP achieves more satisfactory results than LBP and LCVBP. SIFT and SURF perform similarly here, and their performance is worse than those of quaternion-based features. For the average performance of all relations, $QMCBP_q$ surpasses all other methods by different improvements.

C. Texture Classification

The local descriptor has been proven to be a powerful representation for the texture image. In this experiment, we evaluate the proposed descriptors by the texture classification problem. The proposed QMCBP descriptors will be compared with several state-of-the-art local descriptors using following standard color texture data sets respectively: KTH-TIPS 2A [44], KTH-TIPS [44], USPTex [45], Outex TC00013 [46], and Vistex-864 [47]. A summary of these data sets are presented in Table IV, including the class numbers, image numbers for each class, and total image numbers. Fig. 5 provides several examples, and the images on each row are ramdomly selected from these data sets. In order to provide a fair evaluation, the experiment setting for each data set is identical to the previous existing schemes.

1) KTH-TIPS2-a Data Set: This data set totally contains 4395 texture images for eleven materials (such as white bread, cork, cotton, and wool, etc). Each image is a size of 200×200. The images in this data set are captured at nine different scales,

Fig. 5. Texture image examples from different standard datasets. The images in the first to fifth rows are selected from KTH-TIPS 2A, KTH-TIPS, USPTex, Outex TC00013, and Vistex-864 respectively.

TABLE V

CLASSIFICATION RESULTS (PERCENT) OF KTH-TIPS2-a DATA SET. BEST RESULTS ARE IN BOLD

Methods	KTH-TIPS2-a Data set
LBP [4]	58.2
SIFT [1]	59.5
SURF [3]	62.3
WLD [14]	61.0
LCVBP [43]	61.5
QLBP [29]	61.7
QLRBP [30]	64.5
DRLBP [11]	59.0
DRLTP [11]	62.6
$QMCBP_p$	**71.3**
$QMCBP_q$	68.0

under four varying illumination directions, and three poses respectively. Some example images are shown in the first row of Fig. 5.

This experiment evaluates the proposed descriptors by comparing with following approaches: LBP [4], WLD [14], LCVBP [43], QLBP [29], QLRBP [30], SIFT [1], SURF [3], DRLBP [11], and DRLTP [11], respectively. The experiment is carried out as in [11] and [14]. That is, for each material, three images are randomly chosen from the whole data set to form the training set, and the remaining images are used as the testing set. The classification rate on the testing set is applied to measure the performance of each descriptor. This procedure is repeated four times with different training and testing sets, and the average results over four runs are reported. For the proposed descriptors, the nearest neighbor classifier with l_1-norm is used. Table V illustrates the classification performance of all descriptors. It can be seen that the results of two QMCBP descriptors differ in this situation, and $QMCBP_p$ works better than $QMCBP_q$ by 3.3%. The performance of WLD, LCVBP and QLBP are comparable for this data set, and their classification rates are all about 61%. The DRLTP and SURF method surpass these methods by about two percentages, but their performance is worse than that of QLRBP. The proposed two QMCBP descriptors both significantly outperform other descriptors.

2) KTH-TIPS Data Set: There are 10 classes of texture images in this data set, and 81 images for each class.

TABLE VI

COMPARISON RESULTS (PERCENT) OF KTH-TIPS DATA SET USING DIFFERENT DESCRIPTORS. BEST RESULTS ARE IN BOLD FONT

Methods	KTH-TIPS Data set
CK-1 [48]	86.00
Sparse [49]	84.50
LBP [4]	93.83
SIFT [1]	94.57
SURF [3]	78.02
LCVBP [43]	96.54
WLD [14]	97.28
QLBP [29]	97.41
QLRBP [30]	**98.64**
QMCBP_p	**98.64**
QMCBP_q	98.27

Each image is a size of 200×200. Several example images of this data set are shown in the second row of Fig. 5. In this experiment, the proposed descriptors are compared with the algorithms in [48], [49], LBP [4], SIFT [1], SURF [3], WLD [14], LCVBP [43], QLBP [29], and QLRBP [30], respectively. All approaches are evaluated by the leave-one-out method, namely one image of the data set is used as testing sample, while the rest 809 images form the training set every time. The correct classification rate of 810 tests is reported here, as illustrated in Table VI. We can find that the quaternion-based local descriptors all outperform other algorithms for this data set. QLBP achieves a slight improvement compared with WLD. SURF does not work well in this data set, whose classification rate is much smaller than those of other methods. The classification rates of QLRBP and QMCBP_p are the best among all methods. For the proposed schemes, QMCBP_p obtains more satisfactory performance than QMCBP_q, and their results are both superior to that of QLBP.

3) USPTex Data Set: This data set consists of 191 classes of texture images, and there are 12 images for each class. The size of each image is 128×128. Several texture images are shown in the third row of Fig. 5 as examples. In addition to LBP [4], WLD [14], LCVBP [43], SIFT [1], SURF [3], QLBP [29], and QLRBP [30] methods, the following methods are chosen for comparison: average RGB, LBP+Haralick [50], MSD [51], Multilayer CCR [52], HRF [53], Gabor EEE [54], [55], and shortest graph [56]. The experiment here is conducted as the same settings as in literature, namely two thirds of the whole data set is randomly selected to form the training set, and the rest images are the testing set. The nearest neighbor classifier is used. The classification rate on the testing set is used to evaluate each feature, and the average result of ten runs is reported here. The performance of all methods are illustrated in Table VII. It can be seen that QMCBP_p obtains the best performance for this data set, and surpasses QMCBP_q by more than three percentages. For the quaternion-based methods, QMCBP_p and QMCBP_q both work better than QLBP and QLRBP. Gabor EEE, LCVBP, and WLD obtain higher classification results than QMCBP_q, but their results are less than that of QMCBP_p.

4) Outex TC00013 Data Set: There are totally 1360 texture images with size of 128×128 in this data set, where the number of texture class is 68 and each class incudes 20 images. Several texture images are shown in the fourth row of Fig. 5 as examples. For this data set, the experimental settings and the approaches for comparison are identical to the evaluation of the USPTex data set in Section V-C3. The classification results of all methods are reported in Table VII. We can observe that the performance of all test methods for this data set are different from those for the USPTex data set. Features derived by the shortest graph, WLD and QMCBP_p obtain more satisfactory performance compared with other methods. Among the four quaternion-based descriptors, QMCBP_p obtains an improvement of about ten percentages compared with QLBP, QLRBP, and QMCBP_q, and it also outperforms other methods.

TABLE VII

CLASSIFICATION RESULTS (PERCENT) OF DIFFERENT DESCRIPTORS. BEST RESULTS ARE IN BOLD

Methods	Texture Data Sets		
	USPTex	Outex TC00013	Vistex-864
Average RGB	36.19	76.49	58.78
LBP+Haralick [50]	73.17	77.89	91.59
MSD [51]	51.29	49.83	82.07
Multilayer CCR [52]	82.08	68.50	94.74
HRF [53]	49.86	40.00	58.89
Gabor EEE [54], [55]	92.58	75.86	96.92
Shortest Graph [56]	66.71	88.06	87.72
LBP [4]	87.84	84.66	96.89
SIFT [1]	90.16	78.68	93.15
SURF [3]	88.60	81.07	97.77
LCVBP [43]	92.48	79.66	98.78
WLD [14]	92.34	89.07	98.04
QLBP [29]	84.82	78.19	98.07
QLRBP [30]	86.74	79.17	98.41
QMCBP_p	**94.21**	**91.27**	**99.56**
QMCBP_q	91.03	81.13	98.78

5) Vistex-864 Data Set: This data set contains 54 different textures in total, and there are 16 images for each texture. The size of each image is 128×128, and several example images are shown in the fifth row of Fig. 5. The experiment here is also carried out using the setting and comparison methods of the USPTex data set in Section V-C3. Table VII illustrates the classification results of all approaches. It can be seen that QMCBP_p achieves the most satisfactory performance here. The method, derived by the shortest graph [56], does not work well for this data set. WLD and QLBP obtain similar classification results, and they slightly surpass SURF. The performance of LCVBP and QMCBP_q are better than that of QLRBP. The two proposed QMCBP descriptors both outperform other methods with different improvements.

D. Discussions

Except for the classification performance, the computational complexity is also a significant perspective to evaluate a descriptor. This subsection theoretically analyzes the computational cost of the proposed descriptors. Three representative methods, including LBP, WLD, and SIFT are selected for comparison. Without loss of generality, suppose the size of a color image to be $M \times N$. The computational complexity of LBP, WLD, and SIFT are represented as follows [14]:

$$O_{\text{LBP}} = c_1 MN, \tag{23}$$

$$O_{\text{WLD}} = c_2 MN, \tag{24}$$

$$O_{\text{SIFT}} \approx c_3 (u_1 u_2)(v_1 v_2) MN, \tag{25}$$

where c_1, c_2, and c_3 are constants for the computation complexities of each pixel through additions, divisions, or filtering operations for the corresponding methods. u_1 and u_2 in Eq. (25) are the levels of octave and the scales of each octave respectively. v_1 and v_2 denote the sizes of the convolution masks in the derivation of SIFT. Eqs. (23)-(25) reveal that SIFT has a larger computational complexity than LBP and WLD.

From the derivation of QMCBP descriptors, we can see that it mainly involves four procedures, namely calculating the phase from the CTQ result, sorting the phase in each local region, Michelson contrast extraction, and pattern encoding. Except for the second procedure, the computational complexity of all the rest steps will be c_4MN in total, where c_4 is a constant and has the identical meaning as previous ones. Suppose the sorting is conducted in a local region with size of $w_1 \times w_2$ in size, and then the sorting step will take $w_1 w_2 \log(w_1 w_2)MN$ computational cost. Therefore, the total computational complexity of the QMCBP descriptor is:

$$O_{\text{QMCBP}} = c_4 MN + w_1 w_2 \log(w_1 w_2) MN. \tag{26}$$

Comparing Eq. (26) with Eqs. (23)-(25), we can find that QMCBP has larger computational complexity than LBP and WLD, but it is more efficient than SIFT.

VI. Conclusion

In this paper, we developed QMD as a novel framework to extract local characteristics of color images. Compared with traditional local descriptors, QMD derives the Michelson contrast in the quaternion domain and hence considers both the human perception of the image content and the interactions among different color information. Following this framework, we further proposed two QMCBP descriptors as examples. Different color image classification applications were used to validate the effectiveness of the proposed framework and descriptors, and promising results have been achieved. In the future, there are several valuable directions deserving further investigation to improve the performance of the proposed descriptors: developing other ordering strategies for Michelson contrast extraction, extracting more robust and discriminative features based on the Michelson contrast, and fusing different Michelson-law-based descriptors.

Acknowledgements

The authors would like to sincerely thank the anonymous reviewers for their insightful comments and constructive suggestions that significantly improved the quality of this paper.

References

[1] D. G. Lowe, "Distinctive image features from scale-invariant keypoints," *Int. J. Comput. Vis.*, vol. 60, no. 2, pp. 91–110, 2004.

[2] J.-M. Morel and G. Yu, "ASIFT: A new framework for fully affine invariant image comparison," *SIAM J. Imag. Sci.*, vol. 2, no. 2, pp. 438–469, 2009.

[3] H. Bay, T. Tuytelaars, and L. Van Gool, "SURF: Speeded up robust features," in *Proc. Eur. Conf. Comput. Vis. (ECCV)*, May 2006, pp. 404–417.

[4] T. Ojala, M. Pietikäinen, and T. Mäenpää, "Multiresolution gray-scale and rotation invariant texture classification with local binary patterns," *IEEE Trans. Pattern Anal. Mach. Intell.*, vol. 24, no. 7, pp. 971–987, Jul. 2002.

[5] N. Dalal and B. Triggs, "Histograms of oriented gradients for human detection," in *Proc. IEEE Comput. Soc. Conf. Comput. Vis. Pattern Recognit. (CVPR)*, vol. 1. Jun. 2005, pp. 886–893.

[6] C.-Y. Su and J.-F. Yang, "Histogram of gradient phases: A new local descriptor for face recognition," *IET Comput. Vis.*, vol. 8, no. 6, pp. 556–567, 2014.

[7] K. Hara, K. Inoue, and K. Urahama, "Gradient operators for feature extraction from omnidirectional panoramic images," *Pattern Recognit. Lett.*, vol. 54, pp. 89–96, Mar. 2015.

[8] D. K. Park, Y. S. Jeon, and C. S. Won, "Efficient use of local edge histogram descriptor," in *Proc. ACM Workshops Multimedia*, Nov. 2000, pp. 51–54.

[9] C. S. Won, D. K. Park, and S.-J. Park, "Efficient use of MPEG-7 edge histogram descriptor," *Etri J.*, vol. 24, no. 1, pp. 23–30, Feb. 2002.

[10] M. Subrahmanyam, R. Maheshwari, and R. Balasubramanian, "Local maximum edge binary patterns: A new descriptor for image retrieval and object tracking," *Signal Process.*, vol. 92, no. 6, pp. 1467–1479, Jun. 2012.

[11] A. Satpathy, X. Jiang, and H.-L. Eng, "LBP based edge-texture features for object recognition," *IEEE Trans. Image Process.*, vol. 23, no. 5, pp. 1953–1964, May 2014.

[12] A. K. Jain, *Fundamentals of Digital Signal Processing*. Upper Saddle River, NJ, USA: Prentice-Hall, 1989.

[13] J. Chen, S. Shan, G. Zhao, X. Chen, W. Gao, and M. Pietikainen, "A robust descriptor based on Weber's Law," in *Proc. IEEE Conf. Comput. Vis. Pattern Recognit. (CVPR)*, Jun. 2008, pp. 1–7.

[14] J. Chen *et al.*, "WLD: A robust local image descriptor," *IEEE Trans. Pattern Anal. Mach. Intell.*, vol. 32, no. 9, pp. 1705–1720, Sep. 2010.

[15] Y. Jiang, B. Wang, Y. Zhou, W. Li, and Q. Liao, "Patterns of Weber magnitude and orientation for uncontrolled face representation and recognition," *Neurocomputing*, vol. 165, pp. 190–201, Oct. 2015.

[16] R. Lan, Y. Zhou, and Y. Tang, "Quaternionic Weber local descriptor of color images," *IEEE Trans. Circuits Syst. Video Technol.*, to be published, doi: 10.1109/TCSVT.2015.2492839.

[17] T. A. Ell, "Hypercomplex spectral transforms," Ph.D. dissertation, Univ. Minnesota, Minneapolis, MN, USA, 1992.

[18] T. A. Ell and S. J. Sangwine, "Hypercomplex Fourier transforms of color images," *IEEE Trans. Image Process.*, vol. 16, no. 1, pp. 22–35, Jan. 2007.

[19] C. Zou, K. I. Kou, and Y. Wang, "Quaternion collaborative and sparse representation with application to color face recognition," *IEEE Trans. Image Process.*, vol. 25, no. 7, pp. 3287–3302, Jul. 2016.

[20] P. Denis, P. Carre, and C. Fernandez-Maloigne, "Spatial and spectral quaternionic approaches for colour images," *Comput. Vis. Image Understand.*, vol. 107, nos. 1–2, pp. 74–87, 2007.

[21] C. E. Moxey, S. J. Sangwine, and T. A. Ell, "Hypercomplex correlation techniques for vector images," *IEEE Trans. Signal Process.*, vol. 51, no. 7, pp. 1941–1953, Jul. 2003.

[22] B. Chen, H. Shu, H. Zhang, G. Chen, and L. Luo, "Color image analysis by quaternion Zernike moments," in *Proc. IEEE Int. Conf. Pattern Recognit. (ICPR)*, Aug. 2010, pp. 625–628.

[23] B. J. Chen *et al.*, "Quaternion Zernike moments and their invariants for color image analysis and object recognition," *Signal Process.*, vol. 92, no. 2, pp. 308–318, 2012.

[24] L. Q. Guo and M. Zhu, "Quaternion Fourier–mellin moments for color images," *Pattern Recognit.*, vol. 44, no. 2, pp. 187–195, Feb. 2011.

[25] B. Chen, H. Shu, G. Coatrieux, G. Chen, X. Sun, and J. L. Coatrieux, "Color image analysis by quaternion-type moments," *J. Math. Imag. Vis.*, vol. 51, no. 1, pp. 124–144, 2015.

[26] J. Mennesson, C. Saint-Jean, and L. Mascarilla, "New geometric Fourier descriptors for color image recognition," in *Proc. 17th IEEE Int. Conf. Image Process. (ICIP)*, Sep. 2010, pp. 2685–2688.

[27] Z. Yang and S.-I. Kamata, "Hypercomplex polar Fourier analysis for color image," in *Proc. 18th IEEE Int. Conf. Image Process. (ICIP)*, Sep. 2011, pp. 2117–2120.

[28] L. Guo, M. Dai, and M. Zhu, "Quaternion moment and its invariants for color object classification," *Inf. Sci.*, vol. 273, pp. 132–143, Jul. 2014.

[29] R. Lan, Y. Zhou, Y. Y. Tang, and C. L. P. Chen, "Person reidentification using quaternionic local binary pattern," in *Proc. IEEE Int. Conf. Multimedia Expo (ICME)*, Jul. 2014, pp. 1–6.

[30] R. Lan, Y. Zhou, and Y. Y. Tang, "Quaternionic local ranking binary pattern: A local descriptor of color images," *IEEE Trans. Image Process.*, vol. 25, no. 2, pp. 566–579, Feb. 2016.

[31] A. A. Michelson, *Studies in Optics*. North Chelmsford, MA, USA: Courier Corporation, 1995.
[32] S. Nercessian, S. S. Agaian, and K. A. Panetta, "Multi-scale image enhancement using a second derivative-like measure of contrast," *Proc. SPIE*, vol. 8295, p. 82950Q, Feb. 2012.
[33] E. Peli, "In search of a contrast metric: Matching the perceived contrast of Gabor patches at different phases and bandwidths," *Vis. Res.*, vol. 37, no. 23, pp. 3217–3224, Dec. 1997.
[34] S. DelMarco and S. Agaian, "The design of wavelets for image enhancement and target detection," *Proc. SPIE*, vol. 7351, p. 735103, Apr. 2009.
[35] W. R. Hamilton and W. Rowan, *Elements of quaternions*. London, U.K.: Longmans, Green, Company, 1866.
[36] J. Weeks, R. Lehoucq, and J.-P. Uzan, "Detecting topology in a nearly flat spherical universe," *Classical Quantum Gravity*, vol. 20, no. 8, p. 1529, 2003.
[37] N. Brady and D. J. Field, "Local contrast in natural images: Normalisation and coding efficiency," *Perception*, vol. 29, no. 9, pp. 1041–1055, Sep. 2000.
[38] K. E. A. van de Sande, T. Gevers, and C. G. M. Snoek, "Evaluating color descriptors for object and scene recognition," *IEEE Trans. Pattern Anal. Mach. Intell.*, vol. 32, no. 9, pp. 1582–1596, Sep. 2010.
[39] S.-C. Pei and C.-M. Cheng, "Color image processing by using binary quaternion-moment-preserving thresholding technique," *IEEE Trans. Image Process.*, vol. 8, no. 5, pp. 614–628, May 1999.
[40] A. Ess, B. Leibe, and L. Van Gool, "Depth and appearance for mobile scene analysis," in *Proc. IEEE 11th Int. Conf. Comput. Vis. (ICCV)*, Oct. 2007, pp. 1–8.
[41] J. Lu, X. Zhou, Y.-P. Tan, Y. Shang, and J. Zhou, "Neighborhood repulsed metric learning for kinship verification," *IEEE Trans. Pattern Anal. Mach. Intell.*, vol. 36, no. 2, pp. 331–345, Feb. 2014.
[42] J. Lu, J. Hu, X. Zhou, Y. Shang, Y.-P. Tan, and G. Wang, "Neighborhood repulsed metric learning for kinship verification," in *Proc. IEEE Conf. Comput. Vis. Pattern Recognit. (CVPR)*, Jun. 2012, pp. 2594–2601.
[43] S. H. Lee, J. Y. Choi, Y. M. Ro, and K. N. Plataniotis, "Local color vector binary patterns from multichannel face images for face recognition," *IEEE Trans. Image Process.*, vol. 21, no. 4, pp. 2347–2353, Apr. 2012.
[44] *KTH-TIPS Texture Image Database*, accessed on 2015. [Online]. Available: http://www.nada.kth.se/cvap/databases/kth-tips/
[45] A. R. Backes, D. Casanova, and O. M. Bruno, "Color texture analysis based on fractal descriptors," *Pattern Recognit.*, vol. 45, no. 5, pp. 1984–1992, 2012.
[46] *Outex Texture Image Database*, accessed on 2015. [Online]. Available: http://www.outex.oulu.fi/index.php?page=outex_home
[47] *MIT-Vision Texture (VisTex) Image Database*, accessed on 2015. [Online]. Available: http://vismod.media.mit.edu/vismod/imagery/VisionTexture/vistex.html
[48] B. J. L. Campana and E. J. Keogh, "A compression-based distance measure for texture," *Statist. Anal. Data Mining, ASA Data Sci. J.*, vol. 3, no. 6, pp. 381–398, Dec. 2010.
[49] T. Guha and R. K. Ward, "Image similarity using sparse representation and compression distance," *IEEE Trans. Multimedia*, vol. 16, no. 4, pp. 980–987, Jun. 2014.
[50] A. Porebski, N. Vandenbroucke, and L. Macaire, "Haralick feature extraction from LBP images for color texture classification," in *Proc. 1st Workshops Image Process. Theory, Tools Appl.*, Nov. 2008, pp. 1–8.
[51] G. H. Liu, Z. Y. Li, L. Zhang, and Y. Xu, "Image retrieval based on micro-structure descriptor," *Pattern Recognit.*, vol. 44, no. 9, pp. 2123–2133, Sep. 2011.
[52] F. Bianconi, A.Fernández, E. González, D. Caride, and A. Calviño, "Rotation-invariant colour texture classification through multilayer CCR," *Pattern Recognit. Lett.*, vol. 30, no. 8, pp. 765–773, Jun. 2009.
[53] G. Paschos and M. Petrou, "Histogram ratio features for color texture classification," *Pattern Recognit. Lett.*, vol. 24, nos. 1–3, pp. 309–314, Jan. 2003.
[54] M. A. Hoang, J.-M. Geusebroek, and A. W. M. Smeulders, "Color texture measurement and segmentation," *Signal Process.*, vol. 85, no. 2, pp. 265–275, Feb. 2005.
[55] M. J. Swain and D. H. Ballard, "Color indexing," *Int. J. Comput. Vis.*, vol. 7, no. 1, pp. 11–32, 1991.
[56] J. J. de Mesquita Sá Junior, P. C. Cortez, and A. R. Backes, "Color texture classification using shortest paths in graphs," *IEEE Trans. Image Process.*, vol. 23, no. 9, pp. 3751–3761, Sep. 2014.

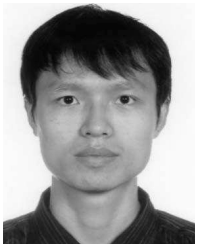

Rushi Lan received the B.S. and M.S. degrees from the Nanjing University of Information Science and Technology, Nanjing, China, and the Ph.D. degree from the University of Macau, Macau, China.

He is currently a Research Assistant with the Department of Computer and Information Science, University of Macau, Macau, China. His research interests include image classification, image denoising, and metric learning.

Yicong Zhou (M'07–SM'14) received the B.S. degree from Hunan University, Changsha, China, and the M.S. and Ph.D. degrees from Tufts University, Massachusetts, USA, all in electrical engineering.

He is currently an Associate Professor and a Director of the Vision and Image Processing Laboratory with the Department of Computer and Information Science, University of Macau, Macau, China. His research interests include chaotic systems, multimedia security, image processing and understanding, and machine learning. He was a recipient of the third price of Macau Natural Science Award in 2014.